

# Evolution of weakly nonlinear short waves riding on long gravity waves

By JUN ZHANG<sup>1</sup> AND W. K. MELVILLE<sup>2</sup>

<sup>1</sup>Ocean Engineering Program, Department of Civil Engineering, Texas A & M University, College Station, TX 77843, USA

<sup>2</sup>R. M. Parsons Laboratory, Department of Civil Engineering, Massachusetts Institute of Technology, Cambridge, MA 02139, USA

(Received 21 October 1988 and in revised form 16 June 1989)

A nonlinear Schrödinger equation, describing the evolution of a weakly nonlinear short gravity wavetrain riding on a longer finite-amplitude gravity wavetrain, is derived. This equation is then used to predict the steady envelope of the short wavetrain relative to the long wavetrain. It is found that approximate analytical solutions agree very well with numerical solutions over a realistic range of wave steepness. The solutions are compared with corresponding studies of the modulation of linear short waves by Longuet-Higgins & Stewart (1960) and Longuet-Higgins (1987). We find that the effect of the nonlinearity of the short waves is to increase the modulation of their wavenumber, significantly reduce the modulation of their amplitude, and reduce the modulation of their slope when compared with the predictions of Longuet-Higgins (1987) for linear short waves on finite-amplitude long waves. The question of the stability of these steady solutions remains open but may be addressed by solutions of this nonlinear Schrödinger equation.

---

## 1. Introduction

The evolution of short wind-generated waves riding on long ocean waves or currents has long been an area of active research in nonlinear wave dynamics. Short waves riding on long waves are modulated by, and interact with, the long waves. They may break on the crest of, and transfer momentum to the long waves. Detailed knowledge is required to understand the processes by which wind energy is transferred to the ocean surface. The recent development of remote sensing from satellites makes it possible to measure the ocean wave spectrum and infer the wind velocity from microwave radar images of the ocean surface (Allan 1983; Stewart 1985). Accurate measurements, however, require more detailed quantitative knowledge of the modulation of short waves, and of energy transfer from the wind to the waves. The demand for this knowledge has stimulated great interest in the study of short- and long-wave interactions in recent years.

The evolution of short wind-generated waves riding on long waves is extremely complicated because it is influenced by the combination of wave-wave interaction and wind-wave interaction. Thus, heuristic models (Keller & Wright 1975; Valenzuela & Wright 1979; Phillips 1984), or assumptions, such as that of a steady short-wave profile, are required in computing the modulation of wind-generated short waves riding on long waves. In order to further understand these processes and establish better models, it is helpful to separate these coupled and complicated processes into their simpler components, and thoroughly study each of them.

Here we concentrate on the steady solution of a weakly nonlinear short gravity wavetrain riding on a finite-amplitude long wave without considering the effects of wind or wave breaking. The stability of the nonlinear short wavetrain riding on a finite-amplitude long wave is currently being studied, and will be presented in a separate paper. Although the short waves are limited to gravity waves and are collinear with the long wave in our study, the method can be extended straightforwardly to include gravity-capillary waves and allow for three-dimensional short waves at the expense of more lengthy algebra.

A striking feature of the modulation of short waves riding on long waves is that the short waves become shorter in wavelength and larger in amplitude at the crests of the long waves, and conversely, longer and smaller at the troughs of the long waves. This phenomenon was first predicted by using the perturbation method (Longuet-Higgins & Stewart 1960), based on the assumption that the short wave is linear and the long wave is weakly nonlinear. The phenomenon was also found in investigating the superharmonic instability of a finite-amplitude periodic wavetrain (Longuet-Higgins 1978). Short waves riding on long waves can be viewed as travelling on currents with a varying horizontal velocity field, provided that the wavelength ratio of short waves to long waves is very small. In this way, Bretherton & Garrett (1968) applied the wave action conservation theory to study the modulation of short waves riding on long waves. Their results confirmed the predictions of Longuet-Higgins & Stewart (1960, 1964). Based on the assumption of small wavelength ratio, Phillips (1981) extended the study of Longuet-Higgins & Stewart (1960) to a long wave with finite amplitude. He applied the wave action conservation theory to a short wave riding on a finite-amplitude long wave. Since the velocity field of a finite-amplitude long wave can be accurately computed through the numerical schemes developed by Schwartz (1974) and Hogan (1980, 1981), the modulation of the short wave can be predicted accurately, with the assumption that the envelope of the short-wave amplitude is steady relative to the long-wave surface. Longuet-Higgins (1987) computed the modulation of short waves riding on a finite-amplitude long wave. His main finding is that the modulation of short waves is much stronger than that predicted by Longuet-Higgins & Stewart (1960). More recently, a canonical Hamiltonian formulation was used to study the dynamics of short waves riding on long waves (Henyey *et al.* 1988). Their results are similar to those of Longuet-Higgins (1987), except that they have extended his calculation to include gravity-capillary waves and allow for a more general two-dimensional long-wave field.

Although the weakly nonlinear limit of the long-wave steepness has been removed in the studies of Phillips (1981), Longuet-Higgins (1987) and Henyey *et al.* (1988), the short wave is still assumed to be linear. In the ocean, short waves riding on a long wave often are not of infinitesimal steepness, even in the absence of wind. Therefore, it is of practical importance to study the modulation of a nonlinear short wavetrain riding on a finite-amplitude long wave. Furthermore, the present study lays the foundation for the investigation of the stability of a short wavetrain riding on a long wave, and this knowledge is essential to justify the assumption that the profile of the short-wave amplitude is steady relative to a long wave.

The short wavetrain is assumed to be weakly nonlinear, and the free-surface boundary conditions are expanded about the surface of the finite-amplitude long wave. Using the perturbation method, a nonlinear Schrödinger equation (equation (3.5)) describing the evolution of a short wavetrain riding on a long wave is derived. We show that the conservation of short-wave action may be reproduced from (3.5)

if the higher-order terms are neglected. We also show that it is consistent with the ordinary nonlinear Schrödinger equation.

Applying (3.5), we calculate the steady envelope of a nonlinear short wavetrain riding on a finite-amplitude long wave. Particular attention is paid to the effect of the short waves' nonlinearity on the modulation. Our numerical results show that the modulation of a short wavetrain with small wave steepness is close to that of a linear short wavetrain (Longuet-Higgins 1987). With the increase of the short wave steepness, the modulation of the short wavelength along the long wave increases only slightly, while the modulation of the short wave amplitude along the long wave declines significantly; thus the modulation of the steepness of the short wave is reduced. For the purpose of confirming our computation and providing a rational explanation of the differences between the steady solutions for linear and nonlinear short wavetrains, we use both approximate analysis and numerical computation to solve (3.5).

It should be pointed out that in our numerical computation, we exclude the case of the long wave of extreme steepness. This is because the extremely steep long wave may be unstable to local or superharmonic disturbances (Longuet-Higgins 1978; Longuet-Higgins & Cokelet 1978; MacKay & Saffman 1986), and instabilities with a large growth rate may lead to numerical difficulties. Furthermore, steady long waves at extreme steepness may not be physically realizable (Longuet-Higgins & Cokelet 1976).

In §2, we employ orthogonal curvilinear coordinates to study the evolution of a weakly nonlinear short wavetrain riding on a finite-amplitude long wave. Using the perturbation method, (3.5) describing the evolution of a short wavetrain riding on a long wave is derived in §3. In §4, we compute the steady solution of a nonlinear short wavetrain riding on a long wave. Finally, the steady solution of a nonlinear short wavetrain riding on a long wave is compared with that of a corresponding linear short wavetrain.

## 2. Governing equations in orthogonal curvilinear coordinates

### 2.1. *Orthogonal curvilinear coordinates*

We introduced three parameters:  $\epsilon_1$  and  $\epsilon_2$  are the steepnesses of the long wave and short wave (at the trough of the long wave), respectively, and  $\epsilon_3$  denotes the ratio of the short wavelength (at the trough of the long wave) to the long wavelength. Since we are concerned with the evolution of a weakly nonlinear short wavetrain riding on a finite-amplitude long wave, the relationships between these scaling parameters are chosen to be:

$$\epsilon_1 = O(\epsilon_2^{\frac{1}{2}}), \quad \epsilon_3 = O(\epsilon_2^{\frac{3}{2}}). \quad (2.1)$$

From this scaling it is seen that the amplitude of the long wave can be greater than the wavelength of the short wave. Therefore, it is not appropriate to expand the free-surface boundary conditions at the calm water level. With the assumption of a weakly nonlinear short wavetrain, however, it is reasonable to expand them at the long-wave surface. Since the profile and the velocity field of the long wave in the absence of the short wave can be computed numerically, we are able to use the standard perturbation method to solve for the short wave. The method of expanding the free-surface boundary conditions at the long-wave surface was used by Longuet-Higgins (1978). The difference is that the short wave in our study is weakly nonlinear, while the superharmonic disturbances in Longuet-Higgins (1978) are infinitesimal. Particular attention should be paid to examining the degree to which

the profile and the velocity field of the long wave will change owing to the presence of the short wave. When the ratio of the short wavelength to the long wavelength is small enough ( $\epsilon_3 \approx O(\epsilon_1^3)$ ), the change of the long wave, and its feedback effect on the short wave, are found to be negligible. This is discussed in Appendix A.

In order to facilitate the algebra, orthogonal curvilinear coordinates are employed, whose transverse and vertical coordinates are the streamlines and equipotentials of the long wave respectively in the absence of the short wave. The relation between the ordinary rectilinear coordinates and the orthogonal curvilinear coordinates is equivalent to the conformal mapping from the physical plane  $(x, z)$  to the complex potential plane  $(s, n)$ . By mapping, the streamlines and equipotentials of the long wave in the  $(x, z)$ -plane project onto the straight lines in the  $(s, n)$ -plane, respectively, as shown in figure 1. Then  $s$  and  $n$  are given by

$$s = \Phi/|C|, \quad n = \Psi/|C|, \quad (2.2)$$

where  $\Phi$ ,  $\Psi$  and  $C$  are the potential, stream functions and phase velocity of the long wave respectively in the absence of the short wave. Since the scales of  $s$  and  $n$  are different from their corresponding projection lengthscales in the  $(x, z)$ -plane (figure 1), the scale factors  $h_1$  and  $h_2$  are introduced to denote the ratios of  $\Delta s_d/\Delta s$  and  $\Delta n_d/\Delta n$ , where the subscript  $d$  denotes the variable expressed in the physical length, i.e. the length projecting on the  $(x, z)$ -plane. For the water with infinite depth,  $h_1$  and  $h_2$  are equal:

$$h(s, n) = h_1(s, n) = h_2(s, n) = C/U_d(s, n), \quad (2.3)$$

where  $U_d(s, n)$  is the particle velocity of the long wave (in a frame moving at its phase velocity). The derivation of (2.3) may be found in Zhang (1987).

## 2.2. Governing equations

We consider a two-dimensional weakly nonlinear short gravity wavetrain riding on a collinear two-dimensional periodic finite-amplitude long gravity wavetrain in water of infinite depth. Both wavetrains are advancing in the same direction, from left to right. However, the results can be easily extended in a straightforward manner to the case in which the long and short waves are moving in the opposite directions.

The flow is assumed to be incompressible, irrotational. The pressure on the free surface is constant, and the short wave riding on the long wave is assumed to have small steepness. The governing equations for the velocity potential  $\phi(x, z, t)$  and profile  $\zeta(x, t)$  of the short wave riding on the long wave can be expressed in the rectilinear coordinates  $(x, z)$  which are moving at phase velocity of the long wave  $C$ :

$$\phi_t + \frac{1}{2}[(C + \Phi_x + \phi_x)^2 + (\Phi_z + \phi_z)^2] + g(\eta + \zeta \cos \theta) = C_0 \quad \text{at } z = \eta + \zeta \cos \theta, \quad (2.4)$$

$$\cos \theta \zeta_t + [\eta_x + (\cos \theta \zeta)_x](C + \Phi_x + \phi_x) = \Phi_z + \phi_z \quad \text{at } z = \eta + \zeta \cos \theta, \quad (2.5)^\dagger$$

$$\Phi_{xx} + \Phi_{zz} + \phi_{xx} + \phi_{zz} = 0 \quad (-\infty < z < \eta + \zeta \cos \theta), \quad (2.6)$$

$$\Phi_z \rightarrow 0, \quad \phi_z \rightarrow 0 \quad \text{as } z \downarrow -\infty, \quad (2.7)$$

where  $\Phi(x)$  and  $\eta(x)$  are the potential function and the profile of the long wave, and are steady relative to the moving coordinates  $x, z$ .  $\theta$  is the local slope angle of the long wave;  $C_0$  is the Bernoulli constant, and  $g$  is the gravitational acceleration. The subscripts  $x, z$  and  $t$  denote the partial derivatives. The  $z$ -axis is positive upwards with  $z = 0$  fixed at the calm water level. The details are shown in figure 2.

† Notice that  $\zeta(x, t)$  is measured normal to the long-wave surface.

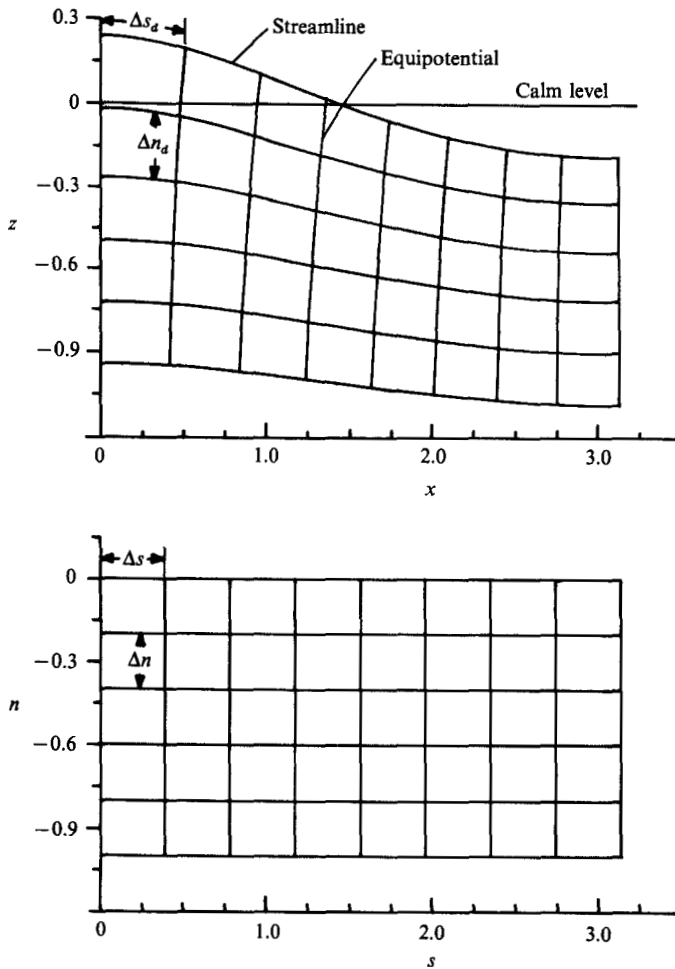


FIGURE 1. The orthogonal curvilinear coordinates.

In the orthogonal curvilinear coordinates defined in §2.1, (2.4)–(2.7) may be written as:

$$\phi_t + \frac{1}{2} \left[ \left( U_d(s, n) + \frac{1}{h} \phi_s \right)^2 + \frac{1}{h^2} \phi_n^2 \right] + g\eta_d(s) + g \cos \theta \zeta h = C_0 \quad \text{at } n = \zeta, \quad (2.8)$$

$$\zeta_t + \frac{1}{h} \zeta_s \left[ U_d(s, n) + \frac{1}{h} \phi_s \right] = \frac{1}{h^2} \phi_n \quad \text{at } n = \zeta, \quad (2.9)$$

$$\frac{\partial}{\partial s} [hU_d(s, n) + \phi_s] + \frac{\partial}{\partial n} \phi_n = 0 \quad (-\infty < n \leq \zeta), \quad (2.10)$$

$$U_d(s, n) \rightarrow C, \quad \phi_n \rightarrow 0 \quad \text{when } n \downarrow -\infty, \quad (2.11)$$

where  $\phi$  is expressed in the physical length, but the subscript  $d$  is dropped to avoid confusion with the derivative subscripts.  $h$  is the scale factor defined in (2.3).  $U_d(s, n)$ ,  $\eta_d(s)$ ,  $C$ , and hence  $h$  can be computed given the wavelength and the amplitude of the long wave. In the following analysis, they are assumed to be known.

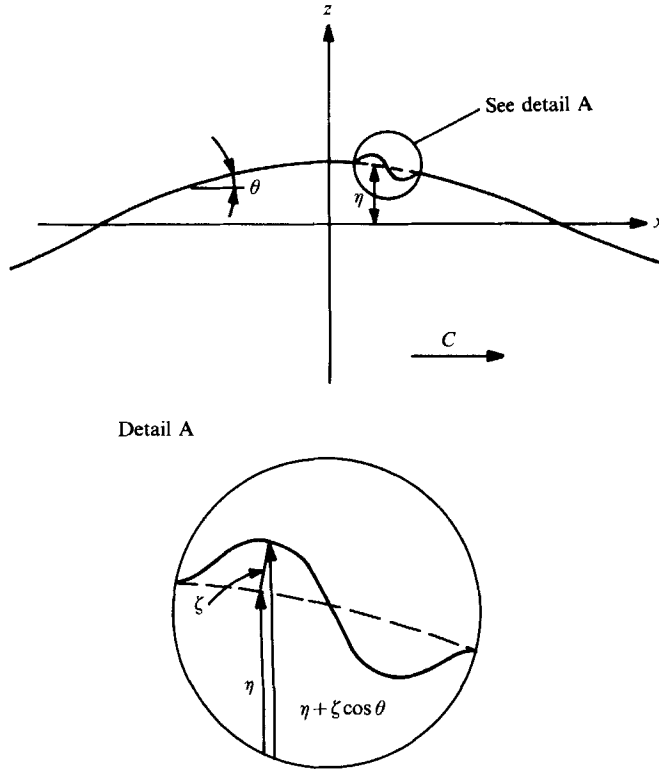


FIGURE 2. Definition sketch for short waves riding on long waves.

2.3. *Expanding equations (2.8) and (2.9) on the long-wave surface*

In expanding (2.8) and (2.9) at the long-wave surface, we assume that the velocity field of the long wave can be analytically extended to the region between  $n = 0$  and  $n = \zeta$ . After subtracting the steady solution of the long wave, we have the following governing equations for the short wave riding on a long wave:

$$\begin{aligned} &\phi_t + H_0 U_0(s) \phi_s + \zeta g_1 + \zeta \phi_{tn} + H_0 U_0(s) \phi_{sn} \zeta + 2H_0 \beta_1 \phi_s \zeta \\ &+ \frac{1}{2} H_0^2 (\phi_s^2 + \phi_n^2) + \frac{1}{2} \phi_{tnn} \zeta^2 + \frac{1}{2} H_0 U_0(s) \phi_{snn} \zeta^2 + 2H_0 \beta_1 \phi_{sn} \zeta^2 \\ &+ \frac{1}{2} H_0 (\phi_s^2 + \phi_n^2)_n \zeta = O(\epsilon_2^3, \epsilon_3^3 \epsilon_2) \zeta g \quad \text{at } n = 0, \end{aligned} \tag{2.12}$$

$$\begin{aligned} &\zeta_t + \zeta_s H_0 U_0(s) - H_0^2 \phi_n + 2\beta_1 H_0 \zeta \zeta_s - 2 \frac{\beta_1}{C} H_0 \zeta \phi_n + H_0^2 (\phi_s \zeta)_s \\ &+ \frac{1}{2} H_0^2 (\phi_{sn} \zeta^2)_s = O(\epsilon_2^3, \epsilon_3^3 \epsilon_2) \zeta \sigma \quad \text{at } n = 0, \end{aligned} \tag{2.13}$$

$$\phi_{ss} + \phi_{nn} = 0 \quad (-\infty < n \leq 0), \tag{2.14}$$

$$\phi_n \rightarrow 0 \quad \text{as } n \downarrow -\infty, \tag{2.15}$$

where

$$H_0 = \frac{1}{h(s, 0)}, \tag{2.16}$$

$$U_0(s) = U_a(s, 0), \tag{2.17}$$

$$\beta_1 = \partial[U_a(s, n)]/\partial n|_{n=0}, \tag{2.18}$$

$$g_1 = g \cos \theta / H_0 + U_0(s) \beta_1, \tag{2.19}$$

$\sigma$  is the intrinsic frequency of the short wave (see §3.2). It may be shown that (2.12) and (2.13) are consistent with the equations derived by Longuet-Higgins (1978, equations (3.1) and (3.4)); this derivation gave only the linear terms of the short wave) to the first order in  $\zeta$  (Zhang 1987).

### 3. Derivation of the nonlinear Schrödinger equation

#### 3.1. Multiple-scale perturbation expansion

The perturbation expansions for  $\phi(s, n, t)$  and  $\zeta(s, t)$  are given by:

$$\phi = \phi^{(0)} + \phi^{(1)} e^{i\bar{\theta}} + * + \phi^{(2)} e^{2i\bar{\theta}} + *, \tag{3.1}$$

$$\zeta = \zeta^{(0)} + \zeta^{(1)} e^{i\bar{\theta}} + * + \zeta^{(2)} e^{2i\bar{\theta}} + *, \tag{3.2}$$

where

$$\partial\bar{\theta}/\partial s = k \quad \text{and} \quad \partial\bar{\theta}/\partial t = -\omega, \tag{3.3}$$

$\bar{\theta}$ ,  $k$  and  $\omega$  are the phase function, wavenumber and frequency of the short wave, respectively, and \* denotes the complex conjugate of the preceding term.  $\phi^{(0)}$  and  $\zeta^{(0)}$  are the long wave potential and amplitude induced by the short wave, and found to be negligibly small.  $\phi^{(1)}$ ,  $\zeta^{(1)}$ ,  $\phi^{(2)}$  and  $\zeta^{(2)}$  represent the short-wave potential, amplitude and their higher harmonics. They may be further expanded with respect to  $\epsilon_2$ . Substituting (3.1)–(3.3) into the governing equations, equations (2.12)–(2.15) may be reduced to a hierarchy of equations according to the order of  $\epsilon_2$  and the harmonics. After solving these equations step by step in increasing order of  $\epsilon_2$ , we obtain the solution for the short wave up to the third order of  $\epsilon_2$ . We then derive the nonlinear Schrödinger equation (3.5). For brevity, the detailed derivation and solution for the short wave are omitted, except where necessary to clarify (3.5). Details may be found in Zhang (1987).

#### 3.2. Amplitude and potential of the leading-order and first-harmonic short wave

$$\phi^{(11)} = -ib e^{kn}, \tag{3.4a}$$

$$\zeta^{(11)} = a, \tag{3.4b}$$

$$b = ag_1/\sigma, \tag{3.4c}$$

$$\sigma^2 = H_0^2 g_1 k, \tag{3.4d}$$

where

$$\sigma = \omega - kH_0 U_0(s), \tag{3.4e}$$

is the intrinsic frequency of the short wave. Equations (3.4d) and (3.4e) are the dispersion relation of the short wave riding on the long wave, and may be transferred to the form expressed in the lengthscale of the original physical plane

$$\sigma^2 = k_d \bar{g}, \tag{3.4f}$$

$$\sigma = \omega - k_d U_0(s), \tag{3.4g}$$

where

$$\bar{g} = H_0 g_1 = g \cos \theta + \frac{1}{2} \frac{\partial [U_0(s)]^2}{\partial n_d}, \tag{3.4h}$$

$$k_d = H_0 k; \tag{3.4i}$$

$k_d$  is the short wavenumber. Equations (3.4f)–(3.4h) are the same as those given by Phillips (1981, equation (2.6)).

## 3.3. The nonlinear Schrödinger equation

The nonlinear Schrödinger equation describing the evolution of a narrow-band short wavetrain riding on a long wave is then given by

$$\begin{aligned} \frac{1}{g_1} \frac{\partial b}{\partial t} + \left[ \frac{H_0^2 C}{g_1} + \frac{H_0^2}{2\sigma} \right] \frac{\partial b}{\partial s} + \frac{H_0^2 C b}{2\sigma} \frac{\partial}{\partial s} \left( \frac{\sigma}{g_1} \right) \\ = -i \left\{ \frac{1}{2\sigma} \left[ \frac{\partial}{\partial t} + H_0^2 C \frac{\partial}{\partial s} \right] \left[ \frac{1}{g_1} \frac{\partial b}{\partial t} + \frac{H_0^2 C}{g_1} \frac{\partial b}{\partial s} \right] + 2 \frac{b^2 b^* k^4 H_0^4}{g_1 \sigma} D \right\}, \end{aligned} \quad (3.5)$$

where 
$$D = 1 + 4 \frac{\beta_1}{\sigma} H_0 \approx 1 + O(\epsilon_1 \epsilon_{\frac{1}{2}}). \quad (3.5a)$$

Neglecting the higher-order terms at the right-hand side of (3.5), some algebraic manipulation gives

$$\frac{\partial}{\partial t} \left[ \frac{|a_d|^2 \bar{g}}{2\sigma} \right] + \frac{\partial}{\partial s_d} \left[ \left( U_0(s) + \frac{\bar{g}}{2\sigma} \right) \frac{|a_d|^2 \bar{g}}{2\sigma} \right] = 0. \quad (3.6)$$

Equation (3.6) is the wave action conservation equation for short waves riding on the long wave. If the envelope of the short-wave amplitude is steady relative to the long-wave surface, then (3.6) becomes

$$\frac{\partial}{\partial s_d} \left[ \left( U_0(s) + \frac{\bar{g}}{2\sigma} \right) \frac{|a_d|^2 \bar{g}}{2\sigma} \right] = 0, \quad (3.7)$$

(cf. Phillips 1981, equation (2.13)).

In the absence of the long wave, the coordinates are stationary in space and the orthogonal curvilinear coordinates degenerate into the rectilinear coordinates. Thus (3.5) may be simplified to

$$\frac{\partial a}{\partial t} + \frac{\sigma}{2k} \frac{\partial a}{\partial x} = -i \left\{ \frac{1}{2\sigma} \frac{\partial^2 a}{\partial t^2} + 2k^2 a^2 a^* \right\}. \quad (3.8)$$

Equation (3.8) is the nonlinear Schrödinger equation describing a narrow-band wavetrain advancing on otherwise calm water.

We may decompose (3.5) into two real equations, with respect to the evolution of the (potential) amplitude  $|b|$  and slow phase function  $\alpha$  of the short wave. Let  $b = |b| e^{i\alpha}$ , multiplying (3.5) by  $b^*$  and then adding and subtracting the product with its complex conjugate respectively, we have the following two equations,

$$\left[ \frac{\partial}{\partial t} + \left( H_0^2 C + \frac{\sigma}{2k} \right) \frac{\partial}{\partial s} \right] |b|^2 = -\frac{\sigma}{k} C |b|^2 \frac{\partial}{\partial s} \left( \frac{\sigma}{g_1} \right) + \frac{g_1}{\sigma} \left[ \frac{\partial}{\partial t} + H_0^2 C \frac{\partial}{\partial s} \right] \left[ \frac{|b|^2}{g_1} \left( \frac{\partial}{\partial t} + H_0^2 C \frac{\partial}{\partial s} \right) \alpha \right]. \quad (3.9a)$$

$$\begin{aligned} \left[ \frac{\partial}{\partial t} + \left( H_0^2 C + \frac{\sigma}{2k} \right) \frac{\partial}{\partial s} \right] \alpha = - \left\{ -\frac{1}{2\sigma} \left[ \left( \frac{\partial}{\partial t} + H_0^2 C \frac{\partial}{\partial s} \right) \alpha \right]^2 \right. \\ \left. + \frac{g_1}{4\sigma |b|^2} \left[ \frac{\partial}{\partial t} + H_0^2 C \frac{\partial}{\partial s} \right] \left[ \frac{1}{g_1} \left( \frac{\partial}{\partial t} + H_0^2 C \frac{\partial}{\partial s} \right) |b|^2 \right] - \frac{1}{8\sigma |b|^4} \left[ \left( \frac{\partial}{\partial t} + H_0^2 C \frac{\partial}{\partial s} \right) |b|^2 \right]^2 + \frac{2|b|^2 k^4 H_0^4}{\sigma} D \right\}. \end{aligned} \quad (3.9b)$$

Equations (35) and (36) of Yuen & Lake (1982) may be recovered from (3.9*a*) and (3.9*b*) if the long wave is absent. The left-hand sides of (3.9*a*) and (3.9*b*) represent the local change of (potential) amplitude  $|b|$  and slow phase  $\alpha$  of the short wave, respectively, for an observer moving at the group velocity of the short wave in the moving coordinates. The right-hand sides show their coupling. Equations (3.9*a*) and (3.9*b*) are used in computing the steady solution (modulation) of a weakly nonlinear short wavetrain riding on a long wave.

#### 4. Computation of the steady solution of the short wave

##### 4.1. Normalization and non-dimensionalization

The normalization is set so that the long wavenumber  $K_d$  and gravity  $g$  are equal to unity, and the coordinate  $s$  ranges from zero to  $2\pi$ . The variations along the long-wave surface, are normalized by the corresponding value at the trough of the long wave. It should be noted that Longuet-Higgins (1987) normalized the variables relative to their corresponding values at the intersection of the calm water level and the long-wave surface. The reason for adopting our normalization is that the coordinate  $s$  at the trough of the long wave is a constant, independent of the steepness of the long wave, while the coordinates at the calm water level of the long-wave surface depend on the long-wave steepness. For the purpose of comparing our results with those of Longuet-Higgins (1987), however, we may transform our normalized variables to his.

The time is non-dimensionalized by the intrinsic frequency of the short wave at the trough of the long wave.

Thus equations (3.9*a*) and (3.9*b*) may become

$$\left\{ \frac{\partial}{\partial \hat{t}} + \frac{\hat{\sigma}}{\hat{k}} [R_c + \frac{1}{2}] \frac{1}{k_0} \frac{\partial}{\partial s} \right\} |\hat{b}|^2 = - \frac{\hat{g}_1 R_c |\hat{b}|^2}{\hat{k} k_0} \frac{\partial}{\partial s} \left( \frac{\hat{\sigma}}{\hat{g}_1} \right) + \frac{\hat{g}_1}{\hat{\sigma}} \left[ \frac{\partial}{\partial \hat{t}} + \frac{\hat{\sigma} R_c}{\hat{k} k_0} \frac{\partial}{\partial s} \right] \left[ \frac{|\hat{b}|^2}{\hat{g}_1} \left( -\bar{\Omega} + \frac{\hat{\sigma}}{\hat{k}} R_c \bar{K} \right) \right], \tag{4.1*a*}$$

$$-\bar{\Omega} + \frac{\hat{\sigma}}{\hat{k}} [R_c + \frac{1}{2}] \bar{K} = - \left\{ -\frac{1}{2\hat{\sigma}} \left[ -\bar{\Omega} + \frac{\hat{\sigma}}{\hat{k}} R_c \bar{K} \right]^2 + \frac{\hat{g}_1}{4\hat{\sigma} |\hat{b}|^2} \left[ \frac{\partial}{\partial \hat{t}} + \frac{\hat{\sigma} R_c}{\hat{k} k_0} \frac{\partial}{\partial s} \right] \left[ \frac{1}{\hat{g}_1} \frac{\partial}{\partial \hat{t}} + \frac{\hat{\sigma} R_c}{\hat{k} \hat{g}_1 k_0} \frac{\partial}{\partial s} \right] |\hat{b}|^2 - \frac{1}{8\hat{\sigma} |\hat{b}|^4} \left[ \frac{\partial |\hat{b}|^2}{\partial \hat{t}} + \frac{\hat{\sigma} R_c}{\hat{k} k_0} \frac{\partial |\hat{b}|^2}{\partial s} \right]^2 + \frac{1}{2} \epsilon_2^2 D_0 \frac{|\hat{b}|^2 \hat{k}^4 \hat{H}_0^4}{\hat{\sigma}} \hat{D} \right\}, \tag{4.1*b*}$$

where the variable with a subscript 0 denotes the value of the corresponding variable at the trough of the long wave, and the variable with a circumflex represents the corresponding normalized variable;

$$\bar{K} = \frac{\partial \alpha}{\partial s} \frac{1}{k_0}, \quad \bar{\Omega} = -\frac{\partial \alpha}{\partial t} \frac{1}{\sigma_0}, \tag{4.2*a, b*}$$

$\bar{K}$  and  $\bar{\Omega}$  are the normalized wavenumber and frequency corrections due to the nonlinearity of the short wave;

$$R_c = C \frac{\sigma}{g_1} \approx O(\epsilon_3^{-\frac{1}{2}}) \tag{4.3}$$

is the phase velocity ratio of the long wave to the short wave;

$$R = \frac{k_{0d}}{K_d} = \epsilon_3^{-1} \quad (4.4)$$

is the wavelength ratio of the long wave to the short wave (at the trough of the long wave). In the following, we drop the circumflexes for simplicity.

#### 4.2. Numerical computation of the long wave

In computing the profile and velocity field of the long wave, we use the numerical scheme developed by Hogan (1980). His scheme allows for surface tension; however, it can also be used in computing gravity waves if the non-dimensional surface tension coefficient is chosen to be negligibly small, say  $10^{-13}$ . Surface profiles of the long wave with respect to its steepness  $\epsilon_1 = 0.05, 0.10, 0.20$  and  $0.30$  are shown in figure 3. The scale factor  $h$  and the gravitational acceleration  $g_1$  may be computed according to (2.3) and (2.19).  $H_0$  and  $g_1$  are shown in figures 4 and 5 as a function of  $s$  and  $\epsilon_1$ . In computing the derivatives with respect to  $s$ , we use the centred difference scheme, whereas the derivative with respect to  $n$  is computed using the high-order backward difference scheme. The magnitude of the intervals  $\Delta s$  and  $\Delta n$  is chosen to be small enough so that the truncation error is smaller than  $10^{-6}$ .

#### 4.3. Steady modulation of a linear short wavetrain

The modulation of a linear short wavetrain riding on a finite-amplitude long wave has been studied numerically by Longuet-Higgins (1987). For the purpose of comparison, it is briefly derived and shown below.

Based on the conservation of the wave phase (assuming that the short wave does not break), and assuming  $k$  is independent of  $t$  (the steady solution), we have a first-order differential equation for  $k$ .

$$\frac{1}{k} \frac{\partial k}{\partial s} = -\frac{2}{H_0} \frac{\partial H_0}{\partial s} - \frac{1}{2g_1[R_c + \frac{1}{2}]} \frac{\partial g_1}{\partial s}. \quad (4.5)$$

Given the wavelength ratio  $R$ , the short wavenumber at the trough of the long wave is determined. Using the centred difference scheme, we may solve (4.5) for  $k$ . Following the same procedure, we may also solve (4.6) for  $\sigma$ .

$$\frac{1}{\sigma} \frac{\partial \sigma}{\partial s} = \frac{1}{2g_1} \frac{\partial g_1}{\partial s} \left\{ 1 - \frac{1}{2[R_c + \frac{1}{2}]} \right\}. \quad (4.6)$$

In order to examine the accuracy of our numerical computation, we have computed the difference between  $\sigma^2$  and  $H_0 g_1 k^2$ . It is found that the maximum absolute error  $|\sigma^2 - H_0 g_1 k^2|$  along the long wave is smaller than  $10^{-6}$  for  $\epsilon_1 = 0.1$  and  $\Delta s = \pi/1024$ . The magnitude of  $k$ ,  $\sigma$  and their derivatives with respect to  $s$  are shown in figures 6–9 as a function of  $s$ , given the wavelength ratio  $R$  and the long-wave steepness  $\epsilon_1$ . It is shown that  $k$  and  $\sigma$  are symmetric, and hence their derivatives with respect to  $s$  are antisymmetric, with respect to the crest and the trough of the long wave.

It is interesting to notice that for moderately steep long waves the normalized wavenumber  $k$  is almost independent of  $R$  but dependent on  $\epsilon_1$ . Figure 10 shows that for the same long-wave steepness, the curves for different wavelength ratios ( $R = 80, 100, 120$ ) are almost identical. This is consistent with Longuet-Higgins (1987, figure 4). The reason for this effective independence of  $R$  is analysed in Appendix B. For the

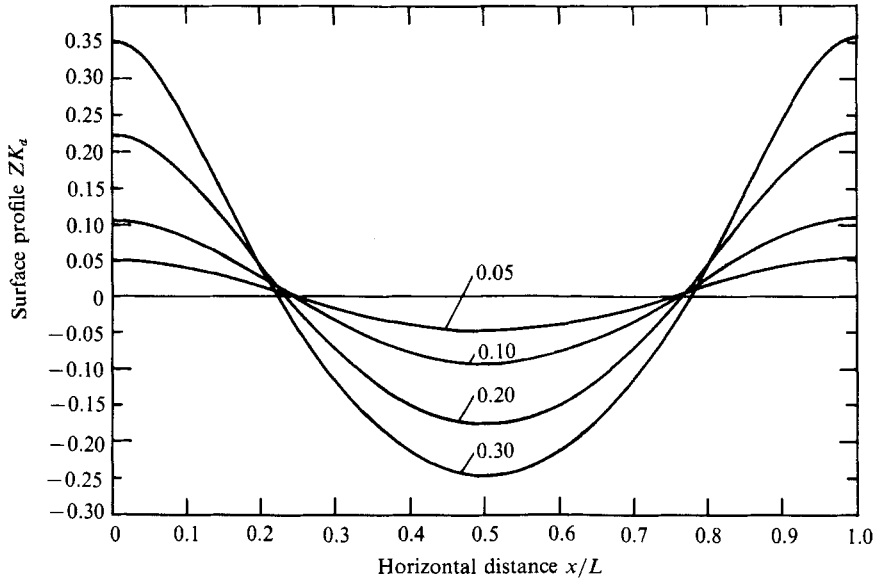


FIGURE 3. Surface elevation of long gravity waves in deep water with wave steepness  $\epsilon_1 = 0.05, 0.10, 0.2$  and  $0.3$ , where  $L$  is the wavelength.

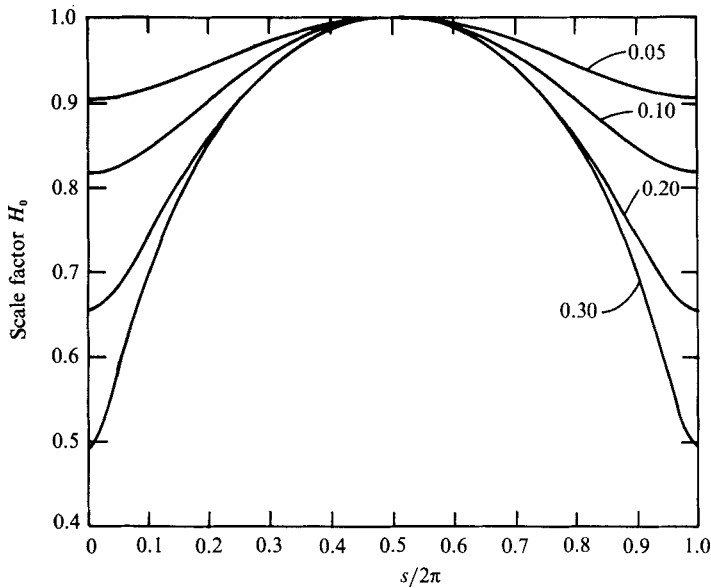


FIGURE 4. The scale factor  $H_0(s)$  defined in (2.16) shown as a function of  $s$  for the long-wave steepness  $\epsilon_1 = 0.05, 0.10, 0.20$  and  $0.30$ .

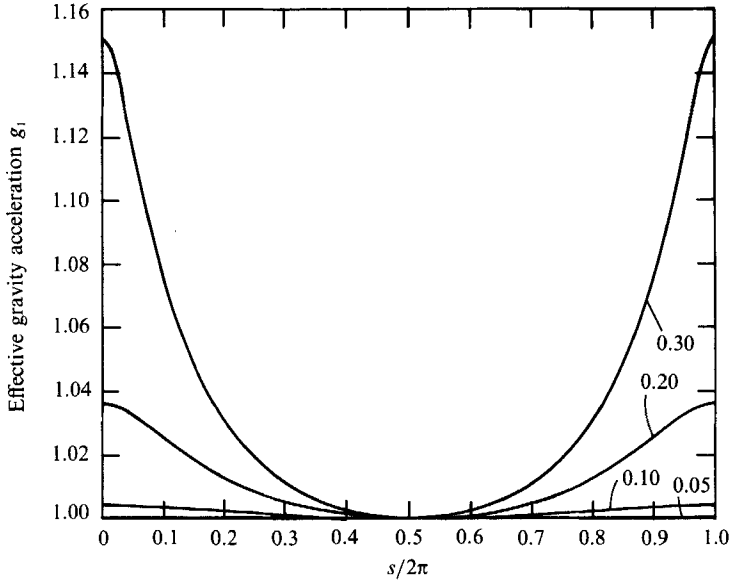


FIGURE 5. The effective gravitational acceleration  $g_1$  defined in (2.19) and normalized by its value at the trough of the long wave, shown as a function of  $s$  for  $\epsilon_1 = 0.05, 0.10, 0.20$  and  $0.30$ .

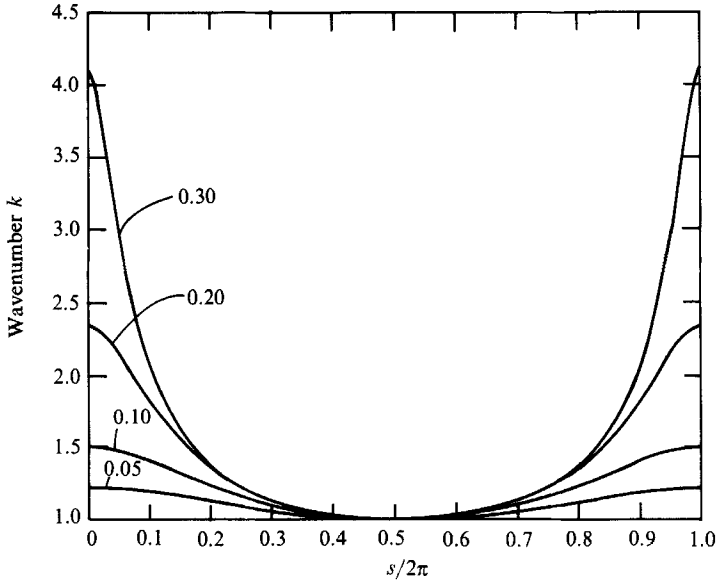


FIGURE 6. The wavenumber  $k$ , normalized by its own value at the trough of the long wave, shown as a function of  $s$ , for  $\epsilon_1 = 0.05, 0.10, 0.20$  and  $0.30$  and the wavelength ratio  $R = 100$ .

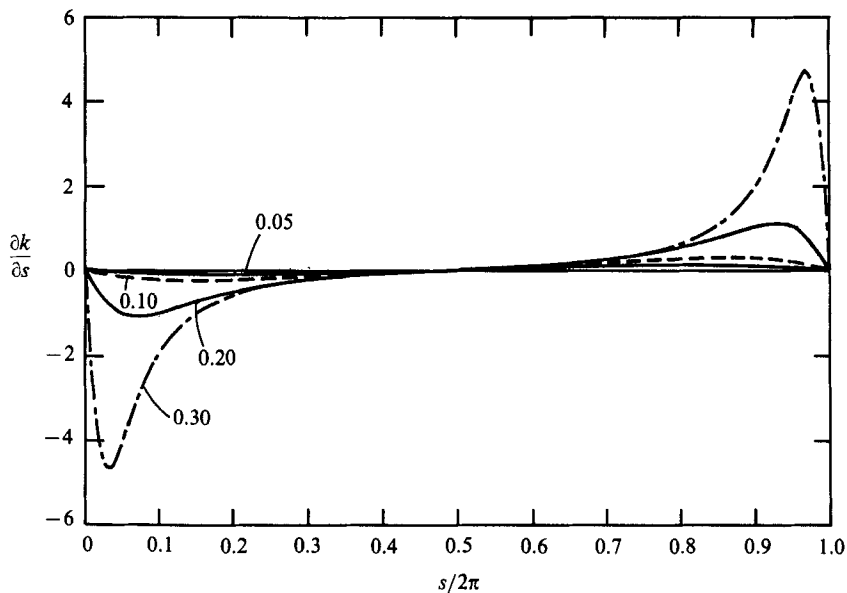


FIGURE 7. The derivative of the normalized wavenumber  $k$  with respect to  $s$ , shown as a function  $s$ , for  $\epsilon_1 = 0.05, 0.10, 0.20$  and  $0.30$  and  $R = 100$ .

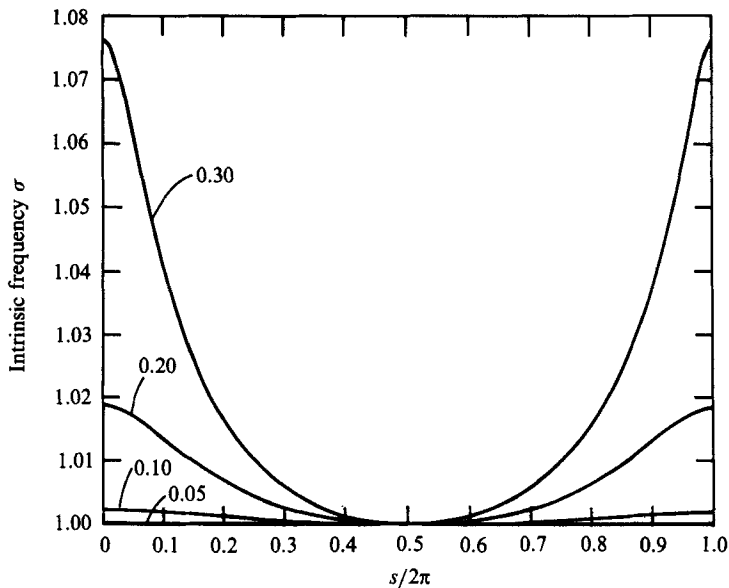


FIGURE 8. The intrinsic frequency  $\sigma$ , defined in (3.4d) and normalized by its own value at trough, shown as a function of  $s$ , for  $\epsilon_1 = 0.05, 0.10, 0.20$  and  $0.30$ , and  $R = 100$ .

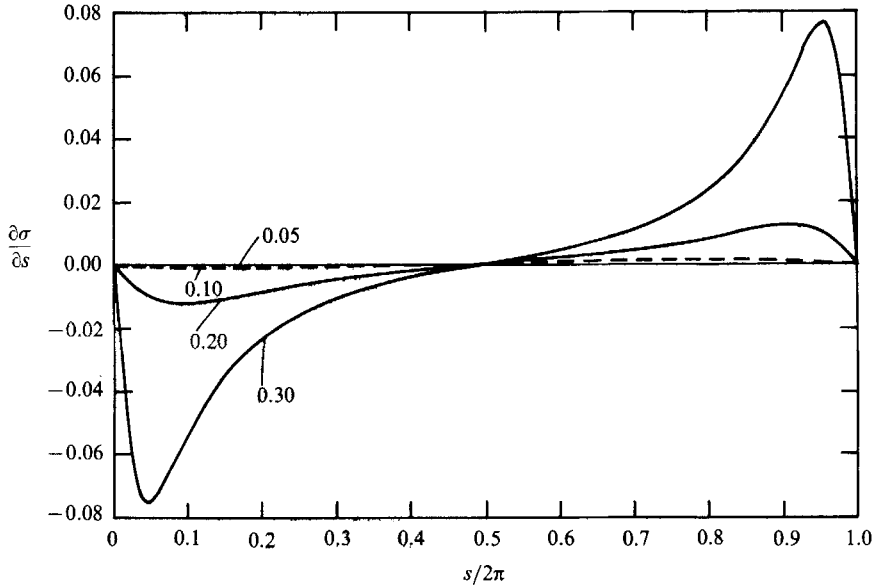


FIGURE 9. The derivative of the normalized intrinsic frequency  $\sigma$  with respect to  $s$ , shown as a function of  $s$ , for  $\epsilon_1 = 0.05, 0.10, 0.20$  and  $0.30$ , and  $R = 100$ .

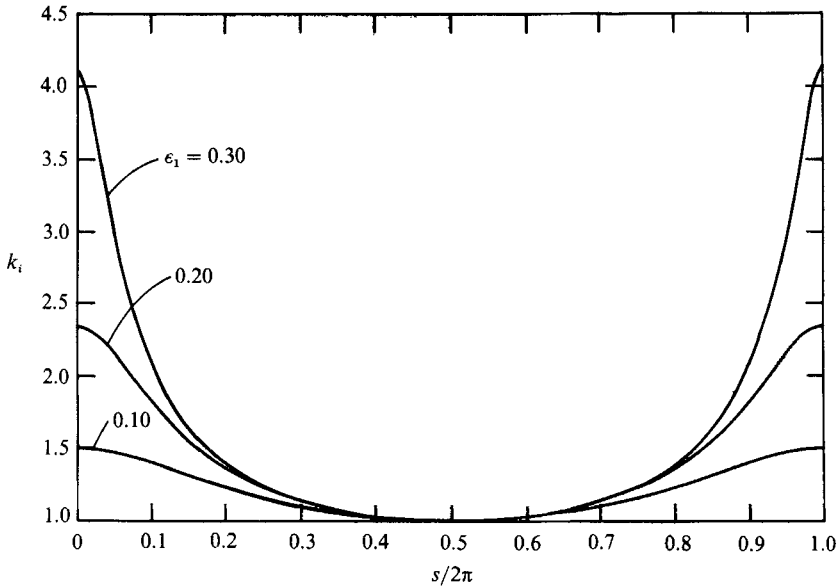


FIGURE 10. The normalized wavenumber  $k_i$  ( $i = 1, 2, 3$ ) with respect to  $R_1 = 80, R_2 = 100, R_3 = 120$ , shown as a function of  $s$  for  $\epsilon_1 = 0.10, 0.20$  and  $0.30$ .

same reason, the variations of the normalized intrinsic frequency  $\sigma$ , and amplitude  $|a_d|$  are also insensitive to  $R$  as long as  $\epsilon_1$  is moderate. Hence, we fix  $R = 100$  in the following numerical computations without significant loss of generality.

The modulation of the normalized amplitude of the steady short wave  $|a_d|$  can be computed from (3.7). For comparison, the normalized wavenumber  $k_d$ , amplitude  $|a_d|$ , and steepness of a steady linear short wavetrain as a function  $x$  with respect to  $\epsilon_1 = 0.10$ , and  $0.20$ , are shown in figures 13–15.

4.4. *Steady modulation of a weakly nonlinear short wavetrain*

In the case of a nonlinear short wavetrain riding on a finite-amplitude long wave, it is expected that its modulation may be different from that of a linear short wavetrain. Hence, we now define the wavenumber and frequency of the short wavetrain by  $k + \bar{K}$  and  $\omega + \bar{\Omega}$  respectively, where  $\bar{K}$  and  $\bar{\Omega}$  are the contribution due to the nonlinearity of the short wave, as shown in (4.2a) and (4.2b). If the short wave is steady relative to the long wave, (4.1a) and (4.1b) may be simplified by letting the time derivatives of  $|b|$ ,  $\bar{K}$  and  $\bar{\Omega}$  equal zero.

$$\frac{\sigma}{k} [R_c + \frac{1}{2}] \frac{1}{k_0} \frac{\partial |b|^2}{\partial s} = -\frac{g_1 |b|^2 R_c}{k k_0} \frac{\partial}{\partial s} \left( \frac{\sigma}{g_1} \right) + \frac{g_1 R_c}{k k_0} \frac{\partial}{\partial s} \left[ \frac{|b|^2}{g_1} \left( -\bar{\Omega} + \frac{\sigma}{k} R_c \bar{K} \right) \right], \quad (4.7a)$$

$$-\bar{\Omega} + \frac{\sigma}{k} (R_c + \frac{1}{2}) \bar{K} = -\left\{ -\frac{1}{2\sigma} \left[ -\bar{\Omega} + \frac{\sigma}{k} R_c \bar{K} \right]^2 + \frac{g_1 R_c}{4k |b|^2 k_0} \frac{\partial}{\partial s} \left[ \frac{\sigma R_c}{k g_1 k_0} \frac{\partial |b|^2}{\partial s} \right] - \frac{\sigma R_c^2}{8k^2 |b|^4 k_0^2} \left( \frac{\partial |b|^2}{\partial s} \right)^2 + \frac{1}{2} \epsilon_2^2 D_0 \frac{|b|^2 K^4 H_0^4}{\sigma} D \right\}, \quad (4.7b)$$

Based on phase conservation and the steady assumption, we may show that  $\partial \bar{\Omega} / \partial s = 0$ ; that is,  $\bar{\Omega}$  is a constant along the long wave surface. Owing to the normalization of the short wavenumber, we let the wavenumber correction  $\bar{K} = 0$  at the trough of the long wave. We find that (4.7a) and (4.7b) are the second-order coupled ordinary differential equations for  $|b|^2$  and  $\bar{K}$  with respect to  $s$ , while  $\bar{\Omega}$  is an unknown constant.

4.4.1. *Approximate analysis*

Before solving (4.7a) and (4.7b) numerically, we present approximate solutions and explore their physical interpretation. From the numerical computation in §§4.2 and 4.3, we find the leading-order term at the right-hand side of (4.7b) is  $\frac{1}{2} \epsilon_2^2 D_0 D (|b|^4 k^4 H_0^4 / \sigma)$  which is  $O(\epsilon_2^2)$ . Neglecting the higher-order terms at the right-hand side of (4.7b), we approximate it by

$$-\bar{\Omega} + \frac{\sigma}{k} (R_c + \frac{1}{2}) \bar{K} = -\frac{1}{2} \epsilon_2^2 D_0 \frac{|b|^2 k^4 H_0^4}{\sigma} D. \quad (4.8)$$

At the trough  $\bar{K} = 0$ , thus

$$\bar{\Omega} = \frac{1}{2} \epsilon_2^2 D_0 \approx O(\epsilon_2^2). \quad (4.9)$$

Since  $\bar{\Omega}$  is a constant, we solve (4.8) for  $\bar{K}$ :

$$\bar{K} = \frac{1}{2} \epsilon_2^2 D_0 \left[ 1 - \frac{|b|^2 k^4 H_0^4}{\sigma} D \right] \frac{k}{\sigma [R_c + \frac{1}{2}]} \approx O(\epsilon_2^2 \epsilon_1 \epsilon_3^{\frac{1}{3}}). \quad (4.10)$$

The result given by (4.9) is clear;  $\bar{\Omega}$  is the frequency correction due to the

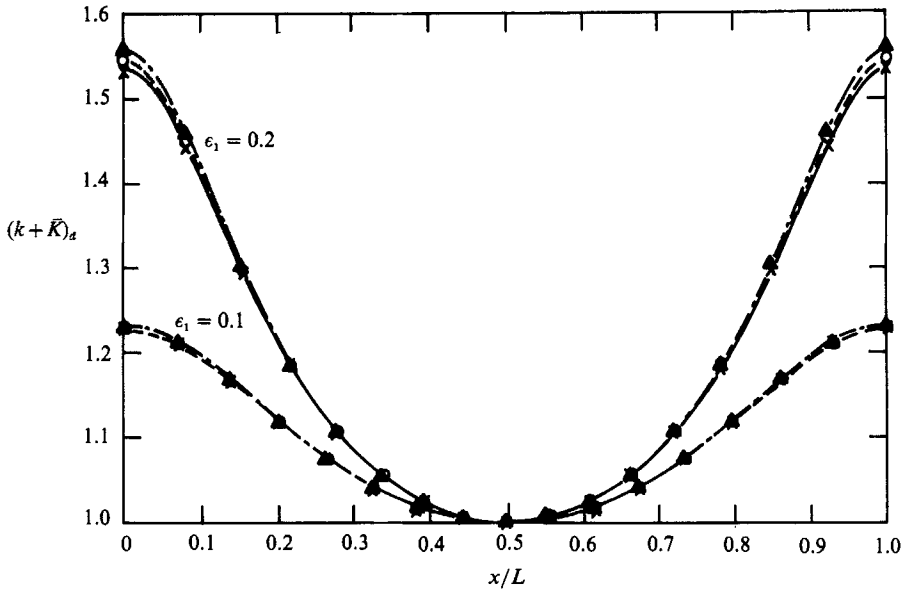


FIGURE 11. The normalized wavenumber  $(k + \bar{K})_a$  of a weakly nonlinear short wavetrain is shown as a function of  $x$ , for  $\epsilon_2 = 0.1, 0.2$  and  $0.3$ ,  $\epsilon_1 = 0.1$  and  $0.2$ . Results from (4.7a) and (4.7b): —,  $\epsilon_2 = 0.1$ ; ---,  $\epsilon_2 = 0.2$ ; — — —,  $\epsilon_2 = 0.3$ . Results from approximation equation (4.8):  $\times$ ,  $\epsilon_2 = 0.1$ ;  $\circ$ ,  $\epsilon_2 = 0.2$ ;  $\blacktriangle$ ,  $\epsilon_2 = 0.3$ .

nonlinearity of the short wave, corresponding to the frequency increase in the case of a weakly nonlinear gravity wavetrain travelling in otherwise calm water. Equation (4.10) shows that  $\bar{K} > 0$  for all  $s$  except at the trough of the long wave. This results from the fact that the steepness of a modulated short wavetrain changes along the long-wave surface. For a gravity wave, its group velocity increases slightly with the increase of its steepness. Hence, the modulated short wavetrain has a larger/smaller group velocity near the crest/trough of the long wave. Owing to its non-uniform group velocity, a modulated short wavetrain is compressed/stretched while riding on the forward/backward face of the long wave. This effect is similar to, but much weaker than, the effect of the particle velocity of the long wave on the short wavetrain. Hence, the variation of  $\bar{K}$  along the long wave is similar to that of  $k$ , and its magnitude is much smaller than the latter. The wavenumber  $(k + \bar{K})_a$  as a function of  $x$ , for  $\epsilon_2 = 0.1, 0.2$  and  $0.3$  and  $\epsilon_1 = 0.1$  and  $0.2$ , is shown in figure 11.

Based on the order of magnitude analysis in (4.9) and (4.10), and the numerical computation in §§4.2 and 4.3, we find the leading-order terms at the right-hand side of (4.7a) are

$$\frac{g_1 R_c}{k k_0} \frac{\partial}{\partial s} \left[ \frac{|b|^2}{g_1} \left( -\bar{\Omega} + \frac{\sigma}{k} R_c \bar{K} \right) \right], \quad -\frac{g_1 R_c |b|^2}{k k_0} \frac{\partial}{\partial s} \left( \frac{\sigma}{g_1} \right),$$

which are  $O(\epsilon_2^2 \epsilon_1 \epsilon_3^{\frac{1}{3}})$  and  $O(\epsilon_2^3 \epsilon_3^{\frac{1}{3}})$ , respectively. Using (4.8) and (4.10) and neglecting the higher-order terms, (4.7a) may be approximated by

$$\frac{\partial}{\partial s} \left[ \left( R_c + \frac{1}{2} \right) |b|^2 \left( 1 + \frac{1}{2} \epsilon_2^2 \alpha^2 k^2 \right) \right] = 0. \tag{4.11}$$

For exploring the physics in (4.11), we transfer it to the form expressed in the original physical lengthscale (cf. §3.2).

$$\frac{\partial}{\partial s} \left\{ \left[ U_0(s) + \frac{\sigma}{2k_d} \right] \frac{|a_d|^2 \bar{g}}{\sigma} \left( 1 + \frac{1}{2} a^2 k^2 \right) \right\} = 0. \quad (4.12)$$

Equation (4.12) is essentially a weakly nonlinear version of wave action conservation, if the short wave is steady relative to the long wave. This interpretation of (4.12) is further explored in Appendix C.

As a result of (4.12), the modulation of  $|a_d|$  along the long-wave surface is smaller than that in a corresponding linear short-wave case. The reduction in the modulation of the short-wave amplitude may be explained by comparing (4.12) with its corresponding linear version (3.7). The wave closer to the crest of the long wave has greater 'wave action'  $\frac{1}{2}(|a_d|^2 \bar{g}/\sigma) \cdot (1 + \frac{1}{2} a^2 k^2)$ , owing not only to the larger wave amplitude  $|a_d|$ , as in the linear short-wave case, but also to the larger wave steepness  $ak$ . Consequently, the wave action flux is greater at the crest of the long wave than in the linear-wave case, and the increase of  $|a_d|$  should be smaller.

#### 4.4.2. Numerical computation

We solve the coupled equations (4.7a) and (4.7b) numerically by an iteration method described below.

The solutions of (4.8) and (4.11) are used as the initial input for  $|b|^2$  and  $\bar{K}$ . Taking the advantage of the fact that  $\bar{K} = 0$  at the trough of the long wave and  $|b|^2$ ,  $k$ ,  $\sigma$ ,  $g_1$  and  $H_0$  are symmetric with respect to the trough of the long wave, we obtain a second-order algebraic equation for  $\bar{\Omega}$ .

$$\bar{\Omega} = -\frac{\bar{\Omega}^2}{2} + \frac{R_c^2}{4k_0^2} \frac{\partial}{\partial s} \left( \frac{H_0^2}{g_1} \frac{\partial |b|^2}{\partial s} \right) + \frac{1}{2} \epsilon_2^2 D_0. \quad (4.13)$$

Equation (4.13) is valid only at the trough of the long wave. We may obtain  $\bar{\Omega}$  according to the requirement that  $\bar{\Omega} \ll 1$ . Having obtained  $\bar{\Omega}$ , we solve equation (4.7b) for  $\bar{K}$ . After substituting the new value of  $\bar{\Omega}$  and  $\bar{K}$  into (4.7a), we solve for  $|b|^2$ . In the computation of (4.7a) and (4.7b), the centred difference scheme is used. We calculate the absolute differences of  $|b|^2$  and  $\bar{K}$  between each cycle. If the maximum absolute differences of  $|b|^2$  and  $\bar{K}$  along the long-wave surface are smaller than their respective tolerance errors, say  $10^{-5}$  and  $10^{-7}$ , the iteration will terminate; otherwise, it continues. Typical CPU time for computing  $|b|^2$ ,  $\bar{K}$  and  $\bar{\Omega}$  is about 5 s on VAX8800 machine when  $\epsilon_1 = 0.1$  and  $\epsilon_2 = 0.10$ . For relatively large steepnesses ( $\epsilon_1 = 0.30$ ,  $\epsilon_2 = 0.30$ ), the CPU time is about 8 s.

In computing  $H_0(s)$ ,  $k$ ,  $g_1$  and  $\sigma$ , we obtain better accuracy by adopting a smaller space interval  $\Delta s$ , say  $\Delta s = \pi/1024$ . When we use the iteration method to solve (4.7a) and (4.7b) for  $|b|^2$ ,  $\bar{K}$  and  $\bar{\Omega}$ , however, a smaller  $\Delta s$  does not always guarantee a more accurate result. This is because the factor  $\partial^2 |b|^2 / \partial s^2$  in (4.7b) may amplify large-wavenumber noise, with the largest amplification factor being  $(R_c + \frac{1}{2})^2 / 4k_0^2 (\Delta s)^2$  for each cycle of iteration when the centred difference scheme is used. In order to avoid this effect (i.e. let the amplification factor be no greater than unity), we choose the space interval  $\Delta s \geq |R_c + \frac{1}{2}| / 2k_0 \approx O(\epsilon_3^{\frac{1}{3}})$ . Hence, we must use decimation on the variable arrays such as  $k$ ,  $\partial k / \partial s$ ,  $H_0$ ,  $g_1$  and  $\sigma$ , to increase the space interval to say  $\Delta s = \pi/64$  when solving (4.7a) and (4.7b). Decimation in the space domain is equivalent to a high-wavenumber cutoff (Oppenheim, Wilsky & Young 1985; Oppenheim & Schafer 1975). The Fourier transform of the steady solution ( $|b|^2$  and

$\bar{K}$ ) should not have any substantial components with large wavenumbers if it is to be consistent with our assumption made in deriving (3.5), that  $|b|^2$  and  $\alpha$  vary slowly along the long-wave surface. Therefore, the decimation should not have any significant effect on our numerical computation.

## 5. Numerical results

Figures 11 and 12 compare the results of  $(\bar{K} + k)_a$  and  $|b|$  obtained from the approximate analysis (equations (4.8) and (4.11)) with those from the numerical computation of (4.7*a*) and (4.7*b*). For small values of both short- and long-wave steepness, the discrepancy between the results of the two methods is negligible. With the increase of both steepnesses, the discrepancy increases; however, their qualitative agreement is retained. It should be mentioned that the relative difference of the amplitude  $|a_d|$  between the results of the approximate analysis and the numerical computation is much smaller than that of  $|b|$ , though we do not show this comparison here. The agreement shows that the approximate analysis is adequate and also confirms the numerical computation of (4.7*a*) and (4.7*b*). Consequently, the discussion of the effect of the short-wave nonlinearity on the modulation based on the approximate equations, is relevant and supported by the numerical solutions.

The effects of the short-wave steepness on the modulation of the short wave riding on the long wave are described in figures 13–15. Figures 13, 14 and 15 show the relative variations of the wavenumber, amplitude and steepness of a steady short wavetrain along the long-wave surface respectively. Given the long-wave steepness, the modulation of a short wavetrain with small wave steepness, say  $\epsilon_2 = 0.1$ , is close to that of a linear short wavetrain. Actually, the results for a linear short wavetrain can be reached in the limit as  $\epsilon_2$  goes to zero. With the increase of the short-wave steepness, the shortening of the short wavelength at the crest of the long wave increases slightly, while the increase of the short-wave amplitude at the crest of the long wave declines significantly. Consequently, the steepening of the short waves at the crest of the long wave decreases.

In figures 13–15, it is shown that the maximum/minimum of the wavelength, amplitude and steepness of the short wavetrain always occurs at the crest/trough of the long wave. Therefore, it is of particular interest to compare the modulation results at the crest and the trough of the long wave, predicted by the present study, by Longuet-Higgins (1987), and by Longuet-Higgins & Stewart (1960). Figures 16–18 show the normalized short wavenumber  $(\bar{K} + k)_a$ , amplitude  $|a_d|$ , and wave steepness at the crest and the trough of the long wave as a function of long-wave steepness, predicted by the three methods. For the purposes of comparison, the wavenumber, amplitude and wave steepness are normalized by their corresponding values at the calm water level of the long wave in figures 16–18. The normalized wavenumber and steepness of a linear short wavetrain riding on a finite-amplitude long wave are computed by the method outlined in §4.3. The results have been checked against the corresponding curves of Longuet-Higgins (1987, figures 4 and 6) and are found to be identical. Although the definition of the wavelength ratio in Longuet-Higgins (1987) is slightly different from our definition shown in (4.4), the difference actually has no effect on the numerical computation for the reasons described in Appendix B. For simplicity, we denote the results of a linear short wavetrain riding on a finite-amplitude long wave as the results predicted by Longuet-Higgins (1987).

When the long-wave steepness is small, the results given by all three methods are

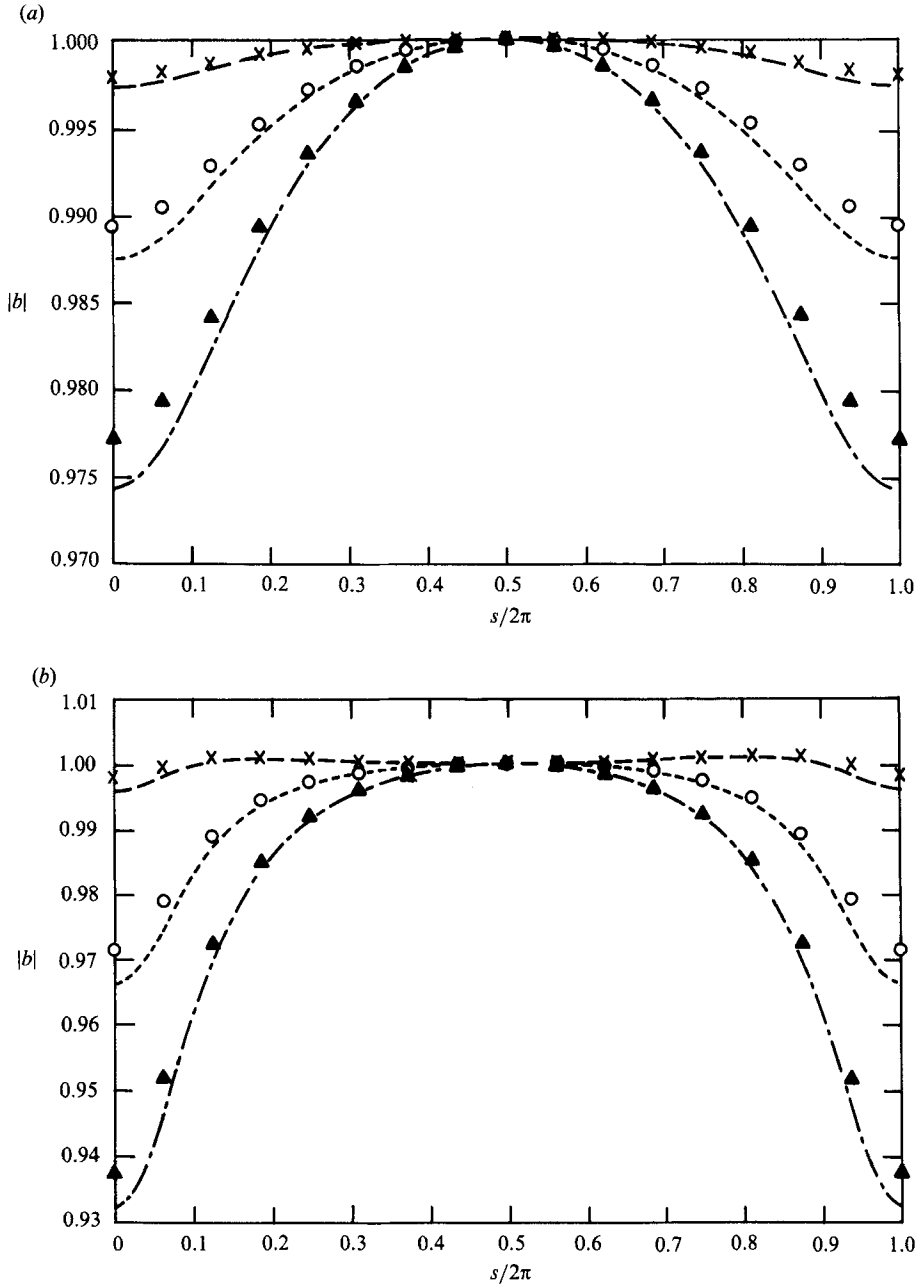


FIGURE 12. (a) The normalized potential amplitude  $|b|$  of a weakly nonlinear short wavetrain is shown as a function of  $s$ , for  $\epsilon_2 = 0.1, 0.2$  and  $0.3$ ,  $\epsilon_1 = 0.1$ . Key as for figure 11. (b) Same as (a), except  $\epsilon_1 = 0.2$ .

very close; no significant differences are observed for  $\epsilon_1 < 0.1$  in figures 16–18. With the increase of the long-wave steepness, however, the results predicted by our study and Longuet-Higgins (1987) begin to depart from those given by Longuet-Higgins & Stewart (1960). This departure is expected, because the latter's prediction is based on the assumption that the long wave is weakly nonlinear. With the increase of the

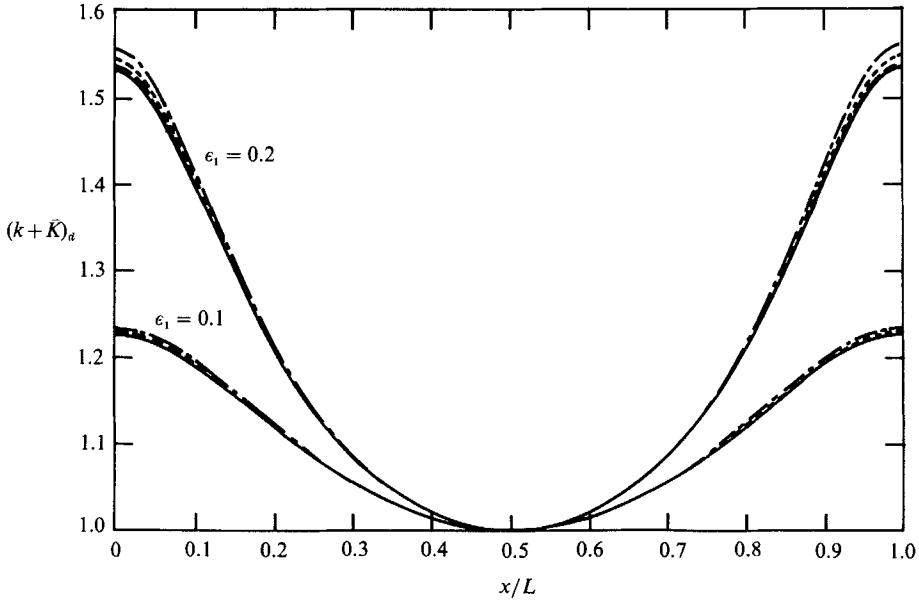


FIGURE 13. The normalized wavenumber  $(k + \bar{K})_d$  of a weakly nonlinear wavetrain, is shown as a function of  $x$  for, —,  $\epsilon_2 = 0.1$ ; ---,  $\epsilon_2 = 0.2$  and - · - ·,  $\epsilon_2 = 0.3$ ,  $\epsilon_1 = 0.1$  and  $0.2$ . For comparison, —, the normalized wavenumber  $k_d$  of a linear wavetrain is also given.

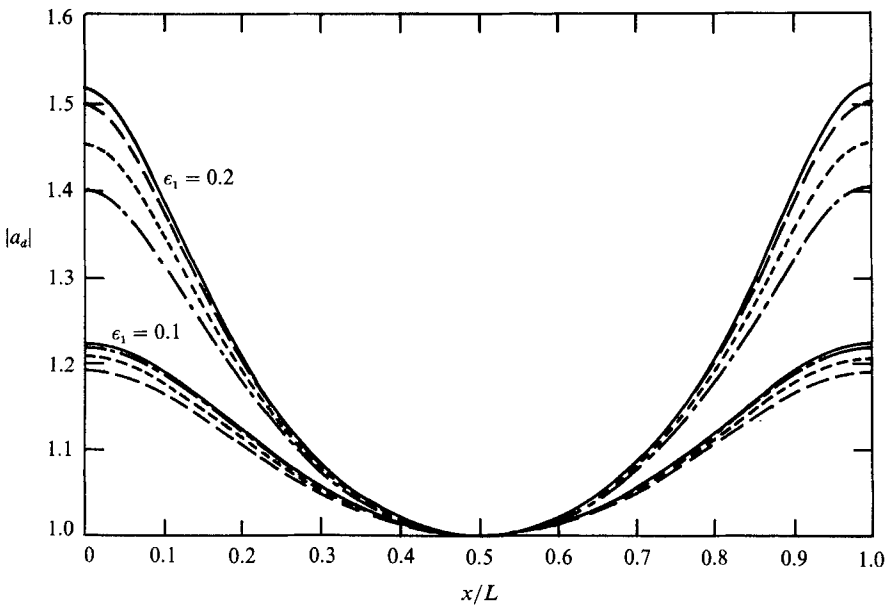


FIGURE 14. The normalized amplitude  $|a_d|$  of a nonlinear wavetrain is shown as a function of  $x$  for, —,  $\epsilon_2 = 0.1$ ; ---,  $\epsilon_2 = 0.2$  and - · - ·,  $\epsilon_2 = 0.3$ ,  $\epsilon_1 = 0.1$  and  $0.2$ . For comparison, —, the normalized amplitude  $|a_d|$  of a linear wavetrain is also given.

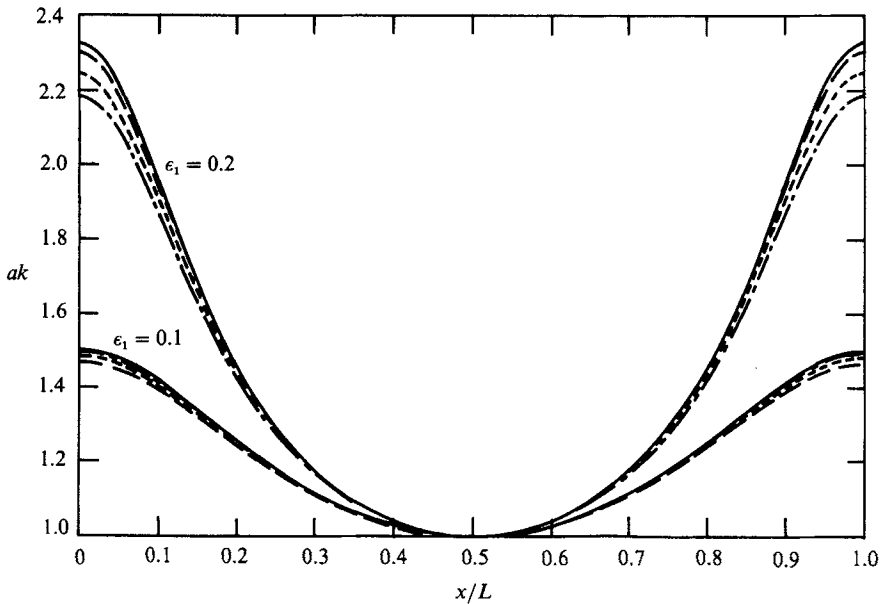


FIGURE 15. The normalized steepness of a nonlinear wavetrain is shown as a function of  $x$  for, ———,  $\epsilon_2 = 0.1$ ; - - -,  $\epsilon_2 = 0.2$  and ·····,  $\epsilon_2 = 0.3$ ,  $\epsilon_1 = 0.1$  and  $0.2$ . For comparison, —, the normalized steepness of a linear wavetrain is also given.

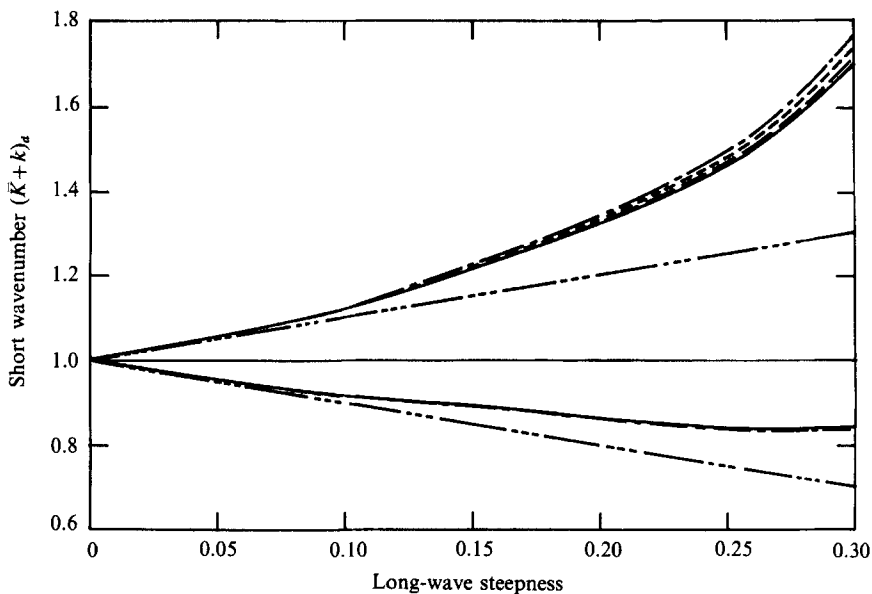


FIGURE 16. The increase/decrease of the short wavenumber  $(\bar{K} + k)_s$  at the crest/trough of the long wave, with respect to the corresponding value at the calm water level, is shown as a function of the long-wave steepness, where — and - - - are the results given by Longuet-Higgins (1987) and Longuet-Higgins & Stewart (1960) respectively; ———, - - - and ····· are our results for  $\epsilon_2 = 0.1, 0.2$  and  $0.3$ .

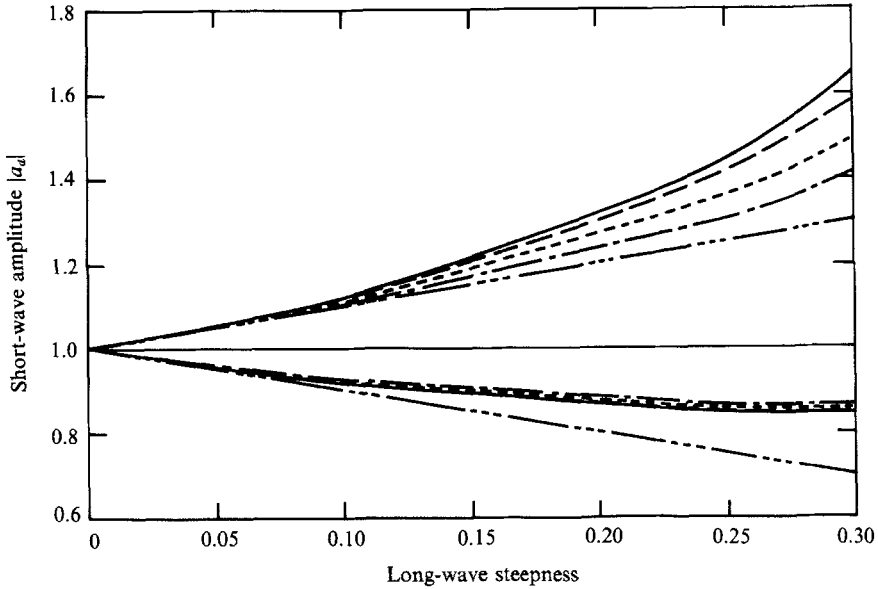


FIGURE 17. The increase/decrease of the short-wave amplitude  $|a_d|$  at the crest/trough of the long wave, with respect to the corresponding value at the calm water level, is shown as a function of the long-wave steepness, where the symbols are defined in figure 16.

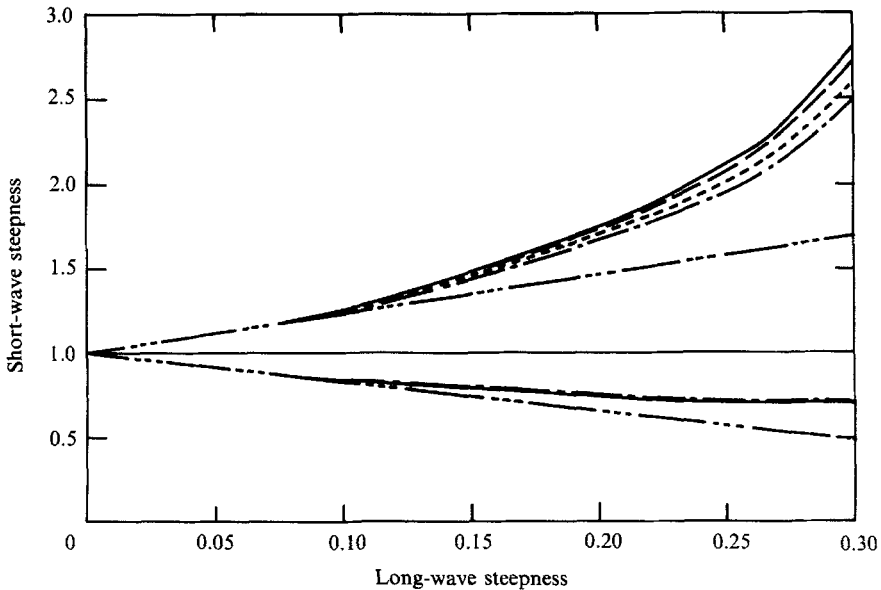


FIGURE 18. The increase/decrease of the short-wave steepness at the crest/trough of the long wave, with respect to the corresponding value at the calm water level, is shown as a function of the long-wave steepness, where the symbols are defined in figure 16.

short-wave steepness, our results begin to differ from those of Longuet-Higgins (1987). This difference may be due to the linear short-wave assumption made in Longuet-Higgins (1987). However, the effects of the short-wave steepness on the shortening/elongation of the short wavelength and on the increase/decrease of the short-wave amplitude at the crest/trough of the long wave are quite different. We describe them below.

With the increase of the short-wave steepness, it is shown in figure 16 that the shortening of the short wavelength at the crest of the long wave is more pronounced, while the elongation of the short wave at the trough is hardly affected. In short, the effect of the short-wave steepness is to enhance the modulation of the short wavelength along the long-wave surface; however, this enhancement is only slight. With the increase of the short-wave steepness, it is shown in figure 17 that the relative increase of the short-wave amplitude at the crest of the long wave declines significantly, while the relative decrease of the short-wave amplitude at the trough is reduced only slightly. Thus the effect of the short-wave steepness is to reduce the modulation of the short-wave amplitude along the long-wave surface. For example, for  $\epsilon_1 = 0.30$  and  $\epsilon_2 = 0.30$ , the relative increase/decrease of the short-wave amplitude at the crest/trough of the long wave is about 45%/12% smaller than that predicted by Longuet-Higgins (1987). As a result of figures 16 and 17, the modulation of the short-wave steepness by the long wave decreases with the increase of the short-wave steepness, as shown in figure 18. For  $\epsilon_1 = 0.30$  and  $\epsilon_2 = 0.30$ , the relative steepening/flattening of the short-wave steepness at the crest/trough of the long wave is about 19%/6% smaller than that predicted by Longuet-Higgins (1987).

This work was supported by National Science Foundation Grants MSM-8514919 and OCE-8614889 to W.K.M. and by the Texas Advanced Technology Research Program under Grant No. 14509 and the NSF Engineering Research Centers under Grant No. CDR-8721512 to J.Z.

### **Appendix A. Change of the long wave due to the presence of the short wave**

The leading order of the zero harmonic short wave (i.e. long wave) is given by

$$\zeta^{(0)} = -\frac{4\beta_1}{\sigma} H_0 |a|^2 k \approx O(\epsilon_1 \epsilon_2 \epsilon_3^{\frac{1}{3}}) a \quad \text{or} \quad O(\epsilon_2^2 \epsilon_3^{\frac{2}{3}}) A, \tag{A 1}$$

where  $A$  is the amplitude of the long wave.

At the crest of the long wave,  $\beta_1 > 0$ , thus  $\zeta^{(0)} < 0$ . At the trough of the long wave,  $\beta_1 < 0$ , and  $\zeta^{(0)} > 0$ . Therefore,  $\zeta^{(0)}$  reduces the amplitude of the long wave. In the dynamic boundary condition,  $g_1 \zeta^{(0)}$  plays the role of an additional pressure. Considering this additional pressure, we examine the changes of the profile and velocity field of the long wave, denoted by  $\Delta\eta_a$  and  $\Delta U_a$  respectively. The dynamic free-surface boundary condition for the long wave may be written as,

$$\frac{1}{2}[U_0(s) + \Delta U_a]^2 + g(\eta_a + \Delta\eta_a) = g_1 \zeta^{(0)} + C_0, \tag{A 2}$$

where

$$\Delta\eta_a = \zeta^{(0)} \cos \theta / H_0. \tag{A 3}$$

Using (2.19) and the steady solution of the long wave, we obtain,

$$U_0(s) \cdot \Delta U_a + \frac{1}{2}(\Delta U_a)^2 = U_0(s) \cdot \beta_1 \zeta^{(0)}. \tag{A 4}$$

To the leading order,

$$\Delta U_a = \beta_1 \zeta^{(0)} \approx O(\epsilon_1^2 \epsilon_2^2 \epsilon_3^3) U_0(s) \quad \text{or} \quad O(\epsilon_1^2 \epsilon_2 \epsilon_3) a\sigma. \quad (\text{A } 5)$$

The corresponding terms neglected in (2.12) and (2.13), are of the order  $O(\epsilon_1^2 \epsilon_2^2 \epsilon_3) ag$  and  $O(\epsilon_1^2 \epsilon_2^2 \epsilon_3) a\sigma$  respectively. In the range of  $\epsilon_1, \epsilon_2, \epsilon_3$  defined in (2.1), their order is higher than  $O(\epsilon_2^3)$ , and hence they may be neglected.

### Appendix B. The relationship between the normalized wavenumber $k$ and the wavelength ratio $R$

Assume that two short wavetrains ride on the same long wave with the normalized wavenumbers  $k_1$  and  $k_2$ , respectively. Their wavelength ratios with respect to the long wave are  $R_1$  and  $R_2$  respectively. According to (4.5),

$$\frac{1}{k_1} \frac{\partial k_1}{\partial s} = -\frac{2}{H_0} \frac{\partial H_0}{\partial s} - \frac{\partial g_1}{\partial s} \frac{1}{2g_1[R_{c_1} + \frac{1}{2}]}, \quad (\text{B } 1)$$

$$\frac{1}{k_2} \frac{\partial k_2}{\partial s} = -\frac{2}{H_0} \frac{\partial H_0}{\partial s} - \frac{\partial g_1}{\partial s} \frac{1}{2g_1[R_{c_2} + \frac{1}{2}]}, \quad (\text{B } 2)$$

where

$$R_{c_i} = C \frac{\sigma_i}{g_1} \left[ H_{00} R_i \frac{g}{g_{10}} \right]^{\frac{1}{2}} \quad (i = 1, 2); \quad (\text{B } 3)$$

$k_1$  and  $k_2$  are normalized by their own value at the trough of the long wave respectively. Subtracting (B 2) from (B 1) then we have

$$\frac{\partial}{\partial s} \ln \left( \frac{k_1}{k_2} \right) = \frac{\partial}{\partial s} (\ln g_1)^{\frac{1}{2}} \left\{ \frac{R_{c_1} - R_{c_2}}{[R_{c_1} + \frac{1}{2}][R_{c_2} + \frac{1}{2}]} \right\}. \quad (\text{B } 4)$$

If both  $R_1$  and  $R_2$  are much greater than unity, an approximate solution for (B 4) is given by

$$\frac{k_1}{k_2} \approx g_1^{\frac{1}{2}(R_1^{\frac{1}{2}} - R_2^{\frac{1}{2}}/R_1^{\frac{1}{2}}R_2^{\frac{1}{2}})}. \quad (\text{B } 5)$$

For a long wave with moderate wave steepness, (B 5) may be approximated by

$$(k_1 - k_2) \approx O \left( \epsilon_1^3 \left[ \frac{R_1^{\frac{1}{2}} - R_2^{\frac{1}{2}}}{R_1^{\frac{1}{2}} R_2^{\frac{1}{2}}} \right] \right). \quad (\text{B } 6)$$

In the case where  $R_1 = 100$ ,  $R_2 = 90$  and  $\epsilon_1 = 0.1$ , it is estimated that the maximum difference between  $k_1$  and  $k_2$  is smaller than  $10^{-5}$ . Thus, we may conclude that the relative variation of the short wavelength along the surface of the long wave with moderate steepness is almost independent of its wavelength ratio with respect to the long wave. Following the same procedure, a similar conclusion may also be drawn in describing the relative variation of the intrinsic frequency and amplitude along the long-wave surface.

### Appendix C. Wave action conservation for a weakly nonlinear wavetrain

Bretherton & Garrett (1969, equation (2.12)) derived the wave action conservation for a wavetrain travelling on a slowly varying current:

$$\frac{d}{dt} (\mathcal{L}_\sigma) + \frac{\partial c}{\partial x} \mathcal{L}_\sigma = 0, \quad (\text{C } 1)$$

where  $\mathcal{L}$  is the average Lagrangian density;  $\sigma$  and  $c$  are the intrinsic frequency and group velocity of the wavetrain, respectively.

If the wavetrain is steady, (C 1) may be written as

$$\frac{\partial}{\partial x}[c\mathcal{L}_\sigma] = 0. \tag{C 2}$$

Bretherton & Garrett (1969, equation (2.25)) proved that

$$\mathcal{L}_\sigma = \frac{E + \mathcal{L}}{\sigma}, \tag{C 3}$$

where  $E$  is energy density.

For a linear wave, the potential energy  $V$  and kinetic energy  $T$  are equal; hence,  $\mathcal{L} = T - V = 0$ .

$$\mathcal{L}_\sigma = \frac{E}{\sigma}. \tag{C 4}$$

However, if we consider a weakly nonlinear wave to the second order,  $\mathcal{L} = T - V > 0$  for gravity waves. Thus

$$\mathcal{L}_\sigma = \frac{E + \mathcal{L}}{\sigma} = \frac{2T}{\sigma}, \tag{C 5}$$

and its kinetic energy  $T$  may be expressed by

$$2T = \frac{1}{2}|a_d|^2 \bar{g} (1 + \frac{1}{2}\alpha^2 k^2). \tag{C 6}$$

Therefore, for long wave-short wave interaction, (C 2) may be written as

$$\frac{\partial}{\partial s_d} \left\{ \left[ U_0(s) + \frac{\sigma}{2k_d} \right] \frac{|a_d|^2 \bar{g}}{\sigma} (1 + \frac{1}{2}\alpha^2 k^2) \right\} = 0,$$

which is equivalent to (4.12).

#### REFERENCES

- ALLAN, T. D. 1983 *Satellite Microwave Sensing*. John Wiley & Sons.
- BREThERTON, F. P. & GARRETT, C. J. R. 1968 Wavetrains in inhomogeneous moving media. *Proc. R. Soc. Lond. A* **302**, 529–554.
- HENYEV, F. S., CREAMER, D. B., DYSTHE, K. B., SCHULT, R. L. & WRIGHT, J. A. 1988 The energy and action of small waves riding on large wave. *J. Fluid Mech.* **189**, 443–462.
- HOGAN, S. J. 1980 Some effects of surface tension on steep water waves. Part 2. *J. Fluid Mech.* **96**, 417–445.
- HOGAN, S. J. 1981 Some effects of surface tension on steep water waves. Part 3. *J. Fluid Mech.* **110**, 381–410.
- KELLER, W. C. & WRIGHT, J. W. 1975 Microwave scattering and the straining of wind-generated waves. *Radio Science* **10**, 139–147.
- LONGUET-HIGGINS, M. S. 1978 The instabilities of gravity waves of finite amplitude in deep water. I. Superharmonic. *Proc. R. Soc. Lond. A* **350**, 526–562.
- LONGUET-HIGGINS, M. S. 1987 The propagation of short surface waves on longer gravity waves. *J. Fluid Mech.* **177**, 293–306.
- LONGUET-HIGGINS, M. S. & COKELET, E. D. 1976 The deformation of steep surface waves on water. I. A numerical method of computation. *Proc. R. Soc. Lond. A* **350**, 1–26.
- LONGUET-HIGGINS, M. S. & COKELET, E. D. 1978 The deformation of steep surface waves on water. II. Growth of normal mode instabilities. *Proc. R. Soc. Lond. A* **364**, 1–28.
- LONGUET-HIGGINS, M. S. & STEWART, R. W. 1960 Changes in the form of short gravity waves on long waves and tidal currents. *J. Fluid Mech.* **8**, 565–583.

- LONGUET-HIGGINS, M. S. & STEWART, R. W. 1964 Radiation stress in water waves, a physical discussion with application. *Deep Sea Res.* **11**, 529–562.
- MACKAY, R. S. & SAFFMAN, P. G. 1986 Stability of water waves. *Proc. R. Soc. Lond.* A **406**, 115–125.
- OPPENHEIM, A. V. & SCHAFER, R. W. 1975 *Digital Signal Processing*. Prentice-Hall.
- OPPENHEIM, A. V., WILLSKY, A. S. & YOUNG, I. T. 1985 *Signal and Systems*. Prentice-Hall.
- PHILLIPS, O. M. 1981 The dispersion of short wavelets in presence of dominant long wave. *J. Fluid Mech.* **107**, 465–485.
- PHILLIPS, O. M. 1984 On the response of the short ocean wave components at a fixed wavenumber to ocean current variations. *J. Phys. Oceanogr.* **14**, 1425–1433.
- SCHWARTZ, L. W. 1974 Computer extension and analytic continuation of Stokes' expansion for gravity waves. *J. Fluid Mech.* **62**, 553–578.
- STEWART, R. H. 1985 *Methods of Satellite Oceanography*. University of California Press.
- VALENZUELA, G. R. & WRIGHT, J. W. 1979 Modulation of short gravity capillary waves by longer periodic flows – a higher order theory. *Radio Science* **14**, 1099–1110.
- YUEN, H. C. & LAKE, B. M. 1982 Nonlinear dynamics of deep-water gravity waves. *Adv. Appl. Mech.* **22**, 67–229.
- ZHANG, J. 1987 Nonlinear interaction between surface water waves. ScD thesis, MIT.